Enhanced escape rate for Hg 254 nm resonance radiation in fluorescent lamps

Enhanced escape rate for Hg 254 nm resonance radiation in fluorescent lamps

James E Lawler[1] and Mark G Raizen[2]

[1] Department of Physics, University of Wisconsin, Madison, WI 53706, USA
[2] Center for Nonlinear Dynamics and Department of Physics, University of Texas, Austin, TX 78712, USA

Abstract
The potential of the low-cost MAGIS isotopic separation method to improve fluorescent lamp efficacy is explored using resonance radiation transport simulations. New Hg isotopic mixes are discovered that yield escape rates for 254 nm Hg I resonance radiation equal to 117% to 122% of the rate for a natural isotopic mix under the same lamp conditions.

(Some figures may appear in colour only in the online journal)

1. Introduction

Fluorescent lighting is the technology of choice for almost all non-residential indoor lighting applications around the world. Compact fluorescent lamps are gaining acceptance in the US mainly for residential use. Concerns about energy efficiency increase year-by-year as evidence strengthens that human activity is driving global climate change. The best modern 4 ft tubular fluorescent lamps, which are the standard for non-residential applications, now achieve 120 lumens per Watt (lpw). Metal-halide high intensity discharge lamps used to light many indoor high-bay areas also have efficacies in the ∼100 lpw range. These efficacies of ∼100 lpw are five or six times better than incandescent lamps.

Further improvements in fluorescent lamp efficacy are desired, but lamp performance appears to be saturating. The promise of solid state lighting is now attracting the attention of lighting researchers. Performance improvements and cost reductions for light-emitting diode (LED) products have been impressive, but costs are still high for many general lighting applications. A 2013 report prepared for the US DoE states[3]: 'In 2012, about 49 million LED lamps and luminaires were installed in the nine applications. LED A-type lamps are about 41% of these installations, but currently only have a penetration rate in this application of less than 1%. LED MR16 lamps have the highest penetration rate at about 10% of all MR16 lamps.' Projections of adoption rates are uncertain and vary widely, but the DoE report states: 'It is forecasted that LED lighting

will represent over 75% of all lighting sales by 2030, resulting in an annual primary energy savings of 3.4 quads.'

Even after inorganic LED and/or organic LED (OLED) technology achieve competitive performance and cost levels, widespread use of fluorescent lighting will likely persist for at least one to two decades due to the many billions of fixtures installed worldwide. Further improvements in fluorescent lighting may be possible by revisiting some old ideas and exploiting some new developments. The improvement in fluorescent lamp performance from tailoring the Hg isotopic mixture, for example by adding ^{196}Hg, was proposed in 1983 (Work and Johnson 1983). This improvement is due to decreased trapping of UV resonance radiation from Hg at 254 nm and thus a decreased probability of collisional quenching of the Hg resonance level. Anderson *et al* (1985) used numerical simulations to explore enhancements of the resonance radiation escape rate from adding ^{196}Hg. Grossman *et al* (1986) experimentally found an improvement of 7% in the UV resonance radiation output from a fluorescent lamp discharge due to an increase of the ^{196}Hg fraction from 0.15% to 2.6%. They noted that the maximum efficacy (in lpw) occurred at lower ^{196}Hg enrichments than the maximum escape rate of UV resonance radiation. They suggested that visible radiation from Hg atoms, e.g. at 546 nm, is affected by a change in the UV resonance escape rate. Indeed the Hg/Ar glow discharge establishes a new steady state when an important process such as the escape of UV resonance radiation is perturbed. Modest but real performance improvements from Hg isotopic tailoring have not yet reached the marketplace due to the prohibitive cost of separating mercury isotopes. The current price of 50% enriched ^{196}Hg is $1655 mg^{-1}, as

---

[3] http://apps1.eere.energy.gov/buildings/publications/pdfs/ssl/led-adoption-report_2013.pdf.

quoted by Oak Ridge National Laboratory. This price is based on the currently available methods of enrichment, which are extremely expensive, placing the use of enriched ^{196}Hg in lamps far outside the range of commercial viability.

It now is time to reconsider Hg isotopic tailoring for fluorescent lamps. The amount of Hg in a standard 4 ft fluorescent lamp has been decreased from ~100 mg in earlier decades to an average of 1.6 mg today. This reduction in Hg dose is being driven by concern over ground water contamination from broken lamps in landfills. Only ~0.05 mg of Hg is in the vapour phase during operation of a 4 ft fluorescent lamp, and some further decrease in the Hg dose is anticipated. The consumption of Hg during lamp operation needed to be tightly controlled and new dosing techniques developed before the Hg dose per lamp could be decreased to 1.6 mg. This reduction in the required amount of separated Hg isotope is quite helpful in any consideration of isotopic tailoring of the lamp dose.

The cost of separating isotopes for a variety of applications will also decrease dramatically due to the invention of the Magnetically Activated and Guided Isotope Separation (MAGIS) technique (Raizen and Klappauf 2012). The case of mercury is particularly well-suited to MAGIS in several ways. The starting point is an effusive beam of mercury, which can be accomplished at a source temperature only slightly above room temperature, hence the kinetic energy of the atoms in the beam is low. The next step in the process is magnetic separation, and the simplest configuration is an array of curved magnetic surfaces, with no line-of-sight between the source and collector. The $6s^2\,^1$S ground state of mercury has $J = 0$, and except for the negligible nuclear spin of odd isotopes, is non-magnetic. Without laser optical pumping to a $J \neq 0$ level, atoms cannot make it through such a curved waveguide without hitting the walls. These walls can be maintained just above the melting point of mercury (234.32 K), so that atoms will stick to a liner, yet flow downwards where they can be collected and not accumulate. A desired isotope of mercury can be separated from this stream by optical pumping to a magnetic $J \neq 0$ state. This can be accomplished with three wavelengths, the first at 253.7 nm to drive the $6s^2\,^1$S$_0$ to $6s6p\,^3$P$_1$ resonance transition, and the others at 404.6 nm and 435.8 nm to optically pump the atoms into the $6s6p\,^3$P$_2$ metastable level via the $6s7s\,^3$S$_1$ level. The polarization can be optimized by pumping the atoms into the $m_j = 2$ 'stretch' state, which is maximally repelled by the magnetic field. In practice, the optical pumping can be accomplished with a narrow-band laser at 253.7 nm, and two blue lasers at 404.6 nm and 435.8 nm respectively. The UV laser is now available with recent advances in optically pumped semi-conductor technology (Paul 2011). The blue wavelengths can be reached with diode lasers in the near-IR, followed by tapered amplifiers, and frequency doubling in an external cavity, or in a periodically poled nonlinear crystal. Laser technology at the desired wavelengths has matured to a point where it is preferred to less efficient lamps.

The economics of fluorescent lamp efficiency improvements from isotopic tailoring of the Hg dose are not difficult to estimate. A 4 ft tubular fluorescent lamp running at ~35 W power input consumes ~700 kWh during its 20 000 h life. Assuming a retail electric energy cost of $0.10 kWh^{-1} such a

lamp consumes $70 of electric energy. A 10% improvement in efficiency would save $7 in operation cost. The incremental cost of an Hg dose with a tailored isotope mix clearly needs to be much less than $7, and should add only modestly to the cost of a lamp. Using the approach studied earlier requires that the 1.6 mg Hg dose be enhanced to 2.6% ^{196}Hg by adding ~0.04 mg of separated ^{196}Hg. This estimate suggests a cost of separated ^{196}Hg of ~$2.50 mg^{-1} or $2500 g^{-1} would add only $0.10 to the lamp cost. The efficiencies inherent in the MAGIS technique indicate that isotope separation at or below this cost per gram are readily achievable.

There is no reason to think that simply enriching the ^{196}Hg isotope automatically yields the best fluorescent lamp dose. If the cost of isotope separation is sufficiently low, then a better optimized isotopic mix will be practical. The next section of this paper reports an expanded study of UV resonance radiation escape rates for various isotopic mixes in Hg/Ar gas mixtures in tubular geometry. Isotopic mixes which yield UV resonance radiation escape rates 17% to 22% higher than that of natural Hg are identified for various tube diameters and buffer gas pressures.

These 17% to 22% enhancements of the UV resonance radiation escape rate are sufficiently large that it should be worth re-optimizing lamp operating conditions, including the Hg density or cold spot temperature, buffer gas density, and discharge current density. Re-optimizations of the discharge operating conditions were not pursued in the earlier studies. Such re-optimizations must be verified through experiments. Fluorescent lamp discharges operate at power densities for which many multi-step excitation and ionization processes are important. Cross sections and rate constant for inelastic collision processes transferring population from one excited level to another and/or resulting in ionization of excited atoms are poorly known. The lack of accurate atomic data involving excited atoms is a problem which necessitates experimental verification. Fluorescent lamps in widespread use today have a variety of discharge currents, tube diameters, and buffer gas pressures with these parameters ranging over roughly an order of magnitude. In this study we have also explored the effect of isotopic tailoring on the 254 nm resonance radiation escape rate in cylindrical systems with 38 mm, 15.9 mm, 50 mm and 6.4 mm diameter and with Ar buffer gas pressures of 2.5 Torr, 2.5 Torr, 0.30 Torr and 5.0 Torr respectively. We found similar, but not identical, optimum Hg isotope mixes for all four cases.

2. Radiation transport code for the 254 nm Hg I transition

Most of the input energy to the positive column of a fluorescent lamp discharge reaches the phosphor coated tube wall as 254 nm resonance radiation from the $6s6p\,^3$P$_1$ to $6s^2\,^1$S$_0$ ground level of Hg. This spin forbidden transition, although two orders of magnitude weaker than the spin allowed 'true' $6s6p\,^1$P$_1$ to $6s^2\,^1$P$_1$ resonance at 185 nm, dominates the power balance of the plasma because of the much lower excitation energy of the $6s6p\,^3$P$_1$ level. Mercury is a sufficiently heavy atom that relativistic effects lead to a partial breakdown of Russell–Saunders (LS) coupling and thus the $6s6p\,^3$P$_1$ level has a small admixture of $6s6p\,^1$P$_1$ character.

The 254 nm transition is sufficiently strong that tens to hundreds of absorption–emission cycles occur while a 254 nm resonance photon migrates to the lamp wall in standard T12 or T8 lamps[4]. This radiation trapping phenomenon is analogous to particle diffusion, but it is correctly modelled using an integral equation rather than a differential equation of a diffusion model. The phenomenon is important in both laboratory and astrophysical plasmas and has been studied for decades (e.g. Biberman 1947, Holstein 1947, Molisch and Oehry 1998 and the many references in their text). Analytic solutions are known for simple line shapes in highly symmetric geometries. The spectral line shape is important because the frequency offset of a photon from the spectral line centre determines the mean-free-path of the photon. It is thus important to include in a realistic fashion the physical processes which redistribute the frequency of a photon during an absorption–emission cycle. There are two commonly used approaches for modelling the change in frequency during an absorption–emission cycle. Complete frequency redistribution (CFR) is appropriate if there is at least one randomizing collision per vacuum radiative lifetime, and partial frequency redistribution (PFR) is appropriate if there is significantly less than one randomizing collision per vacuum radiative lifetime. Under typical fluorescent lamp conditions the CFR approach is satisfactory for the 254 nm resonance line of Hg because the vacuum lifetime of the $6s6p\ ^3P_1$ level is 125 ns (Benck *et al* 1989 and references therein). The PFR approach is needed for the 185 nm resonance line of Hg because the vacuum lifetime of the $6s6p\ ^1P_1$ level is 1.48 ns (Bousquet and Bras 1980 and see Menningen and Lawler 2000 for a comparison of earlier measurements).

For modelling radiation transport with some combination of isotopic and hyperfine structure, a complex geometry, PFR, a spatially and/or temporally varying excited atom production rate per unit volume, it is impractical to use analytic approaches. Either the Propagator Function method (e.g. Lawler *et al* 1993, Parker *et al* 1993) or Monte Carlo simulations are used. The Propagator Function method is best suited for self-consistent discharge simulations because of the speed of the method. Monte Carlo simulations offer the advantages of easier coding and freedom from mesh errors. The Monte Carlo code we use is general purpose in the sense that it includes PFR effects if they are significant. Methods developed by J S Lee (1974, 1977 and 1982) are used in our code as described in Anderson *et al* (1995). Efficient Monte Carlo codes employ the 'Method of Rejection' first described by von Neumann (1951) and sometimes called the 'Null Collision Method'. Monte Carlo codes are common in many fields for both radiation and particle transport. The intricacies of the PFR treatment for radiation transport arise from the fact that the photon frequency has no shift in the absorbing atom's frame but has an angle-dependent Doppler shift viewed from the lab frame during an absorption–emission cycle when no dephasing collisions occurs. (Conservation of energy precludes any frequency shift in the frame of the absorbing atom unless a dephasing collision occurs during

absorption–emission cycle.) Both repeated Doppler shifts and occasional dephasing collisions can move the photon frequency to the spectral line wings where the mean-free-path of the photon is long.

The buffer gas pressures in most fluorescent lamps are in the ∼2 Torr range and the Hg pressure is typically ∼6 mTorr. Electrodeless lamps have lower buffer gas pressure (∼0.3 Torr) and miniature lamps have somewhat higher buffer gas pressure (∼5 Torr), but all three types have similar Hg pressure. Voigt profiles are appropriate for each hyperfine and isotopic component because Doppler broadening dominates spectral line shapes at pressures in the Torr range. There are fast and convenient methods for choosing a random frequency in a Voigt profile and for evaluating a Voigt profile in transport simulations (e.g. Parker *et al* 1993).

Mercury has seven naturally occurring isotopes and two of these have hyperfine structure. Hyperfine and isotopic structure add more complexity to a radiation transport simulation both due to a reduction of the average opacity of the line, and due to collisional effects. Buffer gas collisions randomize the photon frequency across the Voigt profile of the line component of an even isotope and randomize both the upper hyperfine level populations and the frequency in the Voigt profiles of line components from the hyperfine levels of an odd isotope. Resonance collisions involving a ground level and excited Hg atom have the additional 50% probability of isotopic transfer. Menningen and Lawler (2000) described in detail their upgrades of the Anderson *et al* (1995) code to include realistic treatments of collisional transfer process from both buffer gas and resonance collisions in Hg plus rare gas systems.

This radiation transport code was originally developed when personal computers (PCs) had significantly lower CPU clock rates and significantly smaller memory. The code was written for a compiler based on the language FORTH. Because FORTH is a lower level language, it yields quite efficient Monte Carlo codes. A set of 6 Dell Optiplex GX1 PCs with 0.5 GHz clocks and 64 Mbyte of RAM are used to run our radiation transport simulations. These obsolete PCs typically require 12 to 24 h to run a high statistics simulation.

3. Atomic data for 254 nm Hg I transition

The choice of atomic data affects the accuracy of a radiation transport simulation. Herd *et al* (2005) surveyed the atomic data needed to simulate radiation transport of the 254 nm Hg I transition and selected the best available values for the oscillator strength, hypefine and isotopic structure, and dephasing collision rate constants. These selected atomic data are still current. Atomic data choices are discussed briefly in this section and small differences between selected data and those used earlier by Anderson *et al* (1985) are identified. We are building on the earlier work by Anderson *et al* (1985) which explored the effect of increasing the percentage ^{196}Hg and thus need to clarify any differences in selected atomic data for simulations.

Anderson *et al* (1985) likely used a 120 ns vacuum lifetime for the $6sp6p\ ^3P_1$ level as mentioned by Grossman *et al* (1986).

---

[4] Today T8 (1 inch diameter) 4 ft. fluorescent lamps are more popular than the older standard T12 (1.5 inch diameter) 4 ft. fluorescent lamps.

This is within one error bar (5%) of the 125 ns vacuum lifetime recommend by Herd *et al* (2005) based on a measurement by Benck *et al* (1989). The vacuum lifetime of the 6s6p ^{3}P$_1$ level is known to within a few per cent from numerous measurements using a variety of techniques (see the comparison of earlier measurements in Benck *et al* 1989). Anderson *et al* (1985) used the same hyperfine and isotopic structure selected by Herd *et al* (Schweitzer 1963, Gerstenkorn *et al* 1977). It is important to remember that the field shift from the non-negligible nuclear radii dominates the reduced mass shift and yields heavier Hg isotopic components at lower frequency (see the Fabry–Pérot scan of Schweitzer). Except for the isotope shift of the rare ^{196}Hg isotope, all of the hyperfine and isotopic structure is known to better than ±0.001 cm^{-1}. Anderson *et al* used a Voigt parameter (ratio of the Lorentz half width at half max to Doppler half width at *1/e* max) of $a = 0.02$. This agrees well with the Voigt parameter $a = 0.0208$ from the broadening coefficient of $B = 3.2 \times 10^{-10}$ cm^3 s^{-1}±10% (Perrin and Jeanet 1981) for broadening of the 254 nm Hg I transition from Ar collisions selected by Herd *et al* (2005). The much larger broadening coefficient of 3.55×10^{-9} cm^3 s^{-1} mentioned in the Grossman *et al* (1986) paper may be a misprint. Resonance collisions between ground and excited 6s6p ^{3}P$_1$ Hg atoms make only a tiny contribution to the Voigt parameter because the density of Hg is so much lower than the Ar (or other buffer gas) density in a fluorescent lamp. However, resonance collisions do provide a mechanism, in addition to radiative transfer, for moving excitation from one isotope to another. Anderson *et al* (1985) used a value of 1000 Å^2 for the resonance collision cross section. Herd *et al* recommend a temperature independent expression for the resonance collision rate constant based on a realistic quantum calculation supported by experimental tests (Corney 1977). The resonance collision rate is proportional to product of the vacuum decay rate of the 6s6p ^{3}P$_1$ level and the number of ground level Hg atoms per cubic wavelength. This proportionality can be derived using only simple argument about the quantum mechanical sharing of the excitation energy, the superposition of ground and excited states on both atoms, and the subsequent interaction of the transition electric dipoles on both atoms. The resultant collision rate is temperature independent due to the 1/(separation cubed) behaviour of the resonance molecular potential. The proportionality constant is now well known (Corney 1977). The Voigt parameter in the low gas density limit is

$$a_{v0} = \left[4\pi\, \nu_0 \tau_v \sqrt{2k_B T/(Mc^2)}\right]^{-1}$$

where ν_0 is the line centre frequency, τ_v is the vacuum lifetime of the 6s6p ^{3}P$_1$ level, c is the speed of light, k_B is Boltzmann's constant, T is the absolute gas temperature and M is the atomic mass. In this limit of low gas density only radiative broadening contributes to the Lorentz width in the Voigt parameter. The Voigt parameter at finite gas density is

$$a_v = a_{v0}(1 + N_0\, \lambda_0^3\, g_u\, /65.71\, g_l + B\, N_b\, 2\pi\, \tau_v)$$

where N_0 is the density of Hg atoms $\lambda_0 = 253.7279$ nm is the resonance transition wavelength, $g_u = 3$ is the upper level

degeneracy, $g_l = 1$ is the lower level degeneracy, B is the buffer (or foreign) gas broadening coefficient and N_b is the buffer gas density.

4. Resonance radiation escape rates for 254 nm Hg I transition

The Monte Carlo simulation results by Menningen and Lawler (2000) and by Herd *et al* (2005) are all for the fundamental mode decay rate. This 'late time' decay rate is independent of the spatial profile of the excitation rate per unit volume if the source is turned off and the system allowed to relax to the long lived fundamental spatial mode. The spatial distribution of excited atoms in Monte Carlo simulations and in laser-induced fluorescence (LIF) experiments both relax to the fundamental mode at late decay times. The comparisons to LIF experiments reported by Menningen and Lawler for the 185 nm line of Hg I and by Herd *et al* for the 254 nm line (2005) provide confidence that the Monte Carlo code used in this work is realistic and accurate.

In a fluorescent lamp discharge the excitation rate per unit volume likely has a radial variation that at least approximately follows the radial variation of the electron density. Multi-step processes and possible radial variations in the electron energy distribution function can degrade the simple proportionality. It is likely though that the excitation rate per unit volume or source function is similar to the fundamental spatial mode of ambipolar electron–ion diffusion or radiation transport under most circumstances. Anderson *et al* (1985) used a parabolic radial dependence for the source function and reported average escape rates from this source function in their study. This approach makes it much easier to see small effects from changes in isotopic abundances because it is not necessary to wait for late decays and discard ∼90% of each Monte Carlo run. We have adopted the parabolic source function for this work but we note that the radiation escape rate for the fundamental mode of radiation transport is somewhat higher than the average escape rate for the parabolic source function. This is because the parabolic source function excites higher spatial modes of radiation transport with negative amplitude.

Table II in Anderson *et al* (1985) reports resonance radiation escape rates for two cases with cold spot temperatures of 40 °C. The first of these two cases used a natural isotopic mix of Hg, and the second used an isotopic mix with the ^{196}Hg isotope abundance increased to 4%. They found resonance radiation escape rates of $1/(53.7\tau_v)$ for the former case and $1/(49.7\tau_v)$ for the latter based on 120 000 initial photons in each simulation yielding ±0.29% statistical uncertainty. The escape rates in the preceding sentence do not match 44.809 emissions, corresponding to a total decay rate of $1/(44.809\tau_v)$, in their table for the former and 41.948 emissions, corresponding to a total decay rate of $1/(41.948\tau_v)$, in their table for the latter. These differences occur because we have backed out their collisional quenching events. Indeed it is not necessary or desirable to include quenching events in the Monte Carlo simulations. Collisional quenching rates in the plasma are poorly known and such rates can simply be added to the resonance radiation escape rate from a simulation

when quenching needs to be included. We have rerun these two simulations to compare with their results. We find $1/(54.2\tau_v)\pm0.09\%$ for the case with the natural isotopic mix and $1/(49.3\tau_v) \pm 0.28\%$ for the case with ^{196}Hg isotopic fraction increased to 4% as given in the Standard(T12) escape rate column of the first two rows of table 1(*a*). Updated natural or Solar System isotopic abundances from Böhlke *et al* (2005) are used in our simulations. Agreement to within 1% for these two test cases is satisfactory considering the slight differences in input atomic parameters. The lamp parameters in our simulations are nearly identical to those in Anderson *et al* including an Ar density of 8.10×10^{16} cm^{-3} (2.5 Torr at 298 K fill temperature), a Hg density of 1.75×10^{14} cm^{-3} (from a cold spot temperature of $\sim$40 °C), an inner diameter of 38 mm, and an operating gas temperature of 335 K.

The same lamp and atomic parameters are used in all of our simulations reported in the Standard(T12) column of table 1 except that the isotopic composition of the Hg is varied. The simulations in rows 3–9 of the Standard(T12) column confirm the saturation of the escape rate found by Anderson *et al* as the ^{196}Hg fraction is varied from its low natural abundance to 0.16. We note that T12 lamps are the old standard for 4 ft. fluorescent lamps, but it is important to tie our work to the earlier work of Anderson *et al* (1985). Although T8 4 ft. fluorescent lamps are most widely used today, these too are gradually being displaced by smaller diameter T5 lamps. Simulations starting with row 10 of table 1(*b*) onwards are discussed in subsequent paragraphs.

The parameter space of possible isotopic mixes is six dimensional and thus a comprehensive search is challenging. A somewhat selective exploration of the isotopic parameter space is presented in the remainder of table 1. It is clear that even isotopes, particularly ^{202}Hg could be better balanced. The simulations in rows 10–12 of table 1(*b*) explore the effect of better balancing even isotopes. Figure 1 is a plot of the component pattern of the 253.7 nm line with Gaussian (Doppler broadened at 335 K) line shapes for each component. The plot has no optical depth corrections and natural isotopic abundances are used except that the rare ^{196}Hg isotopic component is scaled by $\times$10 to make it visible. Figure 1 shows that the ^{202}Hg and ^{200}Hg components do not overlap each other or hyperfine components of odd isotopes. As indicated by a comparison between row 4 in table 1(*a*) and row 10 in table 1(*b*) of the Standard(T12) column, the effect of balancing the concentration of these two isotopes is quite small. Figure 1 reveals that the under-abundant (natural abundance $\sim$0.0997) even isotope ^{198}Hg component overlaps with the odd isotope hyperfine component 201b. As indicated by a comparison between row 5 in table 1(*a*) and row 11 in table 1(*b*) of the Standard(T12) column, the effect of boosting the concentration of ^{198}Hg is quite small. A comparison between row 5 and row 12 of the Standard(T12) column reveals that the effect of decreasing the concentration of ^{198}Hg is also quite small.

The simulations in rows 13–19 of table 1(*b*) explore isotopic mixes of ^{201}Hg and ^{204}Hg. The 201a hyperfine component is the strongest of the three components from this odd isotope. The overlap of this hyperfine component with the ^{204}Hg component, and a rapid randomization of the

upper ^{201}Hg hyperfine levels suggests that energy absorbed in the excitation of the 6s6p ^{3}P$_1$ level by inelastic collisions of electrons with ^{204}Hg atoms might be transferred to ^{201}Hg via both radiation and resonance collisions and then rapidly escape via radiative emission at the 201b and 201c components. This scheme does not work because the transfer from ^{204}Hg to ^{201}Hg is not sufficiently fast.

The dependence of the escape rate on opacity is illustrated by simulations in rows 20–24 of table 1(*c*). The even isotopes are added one at a time in these simulations and their fractions in the mix are maintained equal. The decrease in opacity with the addition of each even isotope yields an increase in the escape rate, but the effect is not linear.

The simulations in rows 25–32 of table 1(*c*) maintained balanced concentrations of the five even isotopes while increasing the concentration of the ^{201}Hg odd isotope from 0.05 to 0.225. The simulations in rows 29 and 30 yield radiation escape rates higher than can be achieved by simply adding ^{196}Hg as shown in rows 2–9 of the Standard(T12) column of table 1(*a*). Subsequent simulations use these isotopic mixes as starting points for further modification.

These simulations in rows 25–32 of table 1(*c*) did not include any ^{199}Hg and it is thus interesting to explore the effect of reintroducing this odd isotope. The 199A component overlaps with the 201a component and the 199B component overlaps the 201c component. Addition of ^{199}Hg does provide some independent control over relative intensities of the combined overlapping components. However, the simulations of the Standard(T12) column in rows 33–37 of table 1(*d*) indicate that the reintroduction of ^{199}Hg is not helpful.

As mentioned earlier the ^{202}Hg and ^{200}Hg components do not overlap each other or odd isotope hyperfine components. The simulations of the Standard(T12) column in rows 38 and 39 of table 1(*d*) explored the effect of raising and lower concentrations of these two even isotopes in comparison to the other even isotopes and ^{201}Hg. No increase in the radiation escape rate was found compared to the simulations of the Standard(T12) column in rows 29 and 30 of table 1(*c*).

The 254 nm line component of the ^{198}Hg isotope overlaps the 201b component. Simulations reported in rows 40 and 41 of table 1(*e*) explored the effect of varying the ^{198}Hg concentration above and below its value in the simulations of the Standard(T12) column in rows 29 and 30 of table 1(*c*). Changes in the ^{198}Hg concentration did not have much effect.

The 254 nm line component of the ^{204}Hg isotope overlaps the 201a and 199A components. Simulations reported in rows 42–47 of table 1(*e*) explored the effect of varying the ^{204}Hg concentration above and below its value in the simulations of rows 29 and 30 of table 1(*c*). Changes in the ^{204}Hg concentration have a small beneficial effect on the radiation escape rate. The simulation in row 46 of the Standard(T12) column in table 1(*e*) yields the best result of that column with an escape rate 117% of that in row 1 of the Standard column in table 1(*a*) for a natural isotopic mix and 104% of that in rows 5–6 of table 1(*a*) for an optimum addition of the ^{196}Hg isotope to a natural isotopic mix.

Simulations in the T5 or 15.9 mm diameter tube are for an Ar density of 8.23×10^{16} cm^{-3} (2.5 Torr at 293 K fill

Table 1. (*a*) Escape Rate of 254 nm Hg I resonance radiation for various isotopic mixes. The Standard (T12) series has a 38 mm diameter tube, an Ar density of 8.10×10^{16} cm^{-3}, a Hg density 1.75×10^{14} cm^{-3}, and an operating gas temperature of 335 K. The T5 series has a 15.88 mm diameter tube, an Ar density of 8.23×10^{16} cm^{-3}, a Hg density 1.88×10^{14} cm^{-3}, and an operating gas temperature of 335 K. The Electrodeless (T16) series has a 50 mm diameter tube, an Ar density of 9.88×10^{15} cm^{-3}, a Hg density 1.88×10^{14} cm^{-3}, and an operating gas temperature of 335 K. The Miniature (T2) series has a 6.4 mm diameter tube, an Ar density of 1.65×10^{17} cm^{-3}, a Hg density 1.88×10^{14} cm^{-3}, and an operating gas temperature of 335 K. Simulations in the Standard (T12) column of rows 1 and 2 are test cases for comparison to results by Anderson *et al* (1985). Simulations in rows 2 through 9 map the increase and saturation of the 254 nm escape rate with increasing concentration of [196]Hg. (*b*) See the header of table 1(*a*) for an explanation of column headers. Simulations in rows 10 through 12 explore the effect of better balancing the even isotopes. Simulations in rows 13 through 19 explore escape rates for mixes of odd isotope [201]Hg (with hyperfine structure) and even isotope [204]Hg (without hyperfine structure). (*c*) See the header of table 1(*a*) for an explanation of column headers. Simulations in rows 20 through 24 explore the effect of adding even isotopes one by one. Simulations in rows 25 through 32 explore escape rates for mixes with balanced concentrations of the five even isotopes and increasing concentrations of [201]Hg. (*d*) See the header of table 1(*a*) for an explanation of column headers. Simulations in rows 33 through 37 explore the effect of reintroducing some [199]Hg to the mixes in rows 29 and 30 of table 1(*c*). Simulations in rows 38 and 39 explore the effect of raising and lowering the concentration of the isolated even isotopes [200]Hg and [202]Hg starting from the mixes in rows 29 and 30 of table 1(*c*). (*e*) See the header of table 1(*a*) for an explanation of column headers. Simulations in rows 40 and 41 explore escape rates for mixes with increased and decreased [198]Hg starting from the mixes in rows 29 and 30 of table 1(*c*). Simulations in rows 42 through 47 explore escape rates for mixes with increased and decreased [204]Hg starting from the mixes in rows 29 and 30 of table 1(*c*).

	Isotopic fraction							Escape rate			
#	[196]Hg	[198]Hg	[199]Hg	[200]Hg	[201]Hg	[202]Hg	[204]Hg	Standard(T12)	T5	Electrodeless(T16)	Miniature(T2)
(*a*)											
1	0.0015	0.0997	0.1687	0.2310	0.1318	0.2986	0.0687	$1/(54.2\tau_v) \pm 0.09\%$	$1/(24.68\tau_v) \pm 0.08\%$	$1/(99.9\tau_v) \pm 0.06\%$	$1/(9.15\tau_v) \pm 0.07\%$
2	0.0400	0.0959	0.1622	0.2221	0.1267	0.2871	0.0661	$1/(49.3\tau_v) \pm 0.28\%$	$1/(22.48\tau_v) \pm 0.07\%$	$1/(87.9\tau_v) \pm 0.06\%$	$1/(8.50\tau_v) \pm 0.06\%$
3	0.0200	0.0979	0.1656	0.2267	0.1294	0.2931	0.0674	$1/(50.8\tau_v) \pm 0.28\%$	$1/(23.41\tau_v) \pm 0.08\%$	$1/(91.2\tau_v) \pm 0.05\%$	$1/(8.81\tau_v) \pm 0.06\%$
4	0.0600	0.0939	0.1588	0.2175	0.1241	0.2811	0.0647	$1/(48.7\tau_v) \pm 0.25\%$	$1/(21.89\tau_v) \pm 0.07\%$	$1/(86.7\tau_v) \pm 0.05\%$	$1/(8.26\tau_v) \pm 0.06\%$
5	0.0800	0.0919	0.1554	0.2128	0.1214	0.2751	0.0633	$1/(48.3\tau_v) \pm 0.23\%$	$1/(21.49\tau_v) \pm 0.07\%$	$1/(86.3\tau_v) \pm 0.05\%$	$1/(8.08\tau_v) \pm 0.06\%$
6	0.1000	0.0899	0.1521	0.2082	0.1188	0.2691	0.0619	$1/(48.3\tau_v) \pm 0.08\%$	$1/(21.25\tau_v) \pm 0.07\%$	$1/(86.2\tau_v) \pm 0.06\%$	$1/(7.94\tau_v) \pm 0.06\%$
7	0.1200	0.0879	0.1487	0.2036	0.1162	0.2632	0.0605	$1/(48.3\tau_v) \pm 0.08\%$	$1/(21.13\tau_v) \pm 0.07\%$	$1/(86.3\tau_v) \pm 0.09\%$	$1/(7.84\tau_v) \pm 0.04\%$
8	0.1400	0.0859	0.1453	0.1990	0.1135	0.2572	0.0592	$1/(48.3\tau_v) \pm 0.08\%$	$1/(21.07\tau_v) \pm 0.07\%$	$1/(86.5\tau_v) \pm 0.06\%$	$1/(7.78\tau_v) \pm 0.04\%$
9	0.1600	0.0839	0.1419	0.1943	0.1109	0.2512	0.0578	$1/(48.4\tau_v) \pm 0.07\%$	$1/(21.10\tau_v) \pm 0.07\%$	$1/(86.7\tau_v) \pm 0.06\%$	$1/(7.77\tau_v) \pm 0.03\%$
(*b*)											
10	0.0600	0.0939	0.1588	0.2493	0.1241	0.2493	0.0647	$1/(48.7\tau_v) \pm 0.24\%$	$1/(21.85\tau_v) \pm 0.07\%$	$1/(86.7\tau_v) \pm 0.05\%$	$1/(8.22\tau_v) \pm 0.06\%$
11	0.0800	0.1400	0.1464	0.2005	0.1144	0.2591	0.0596	$1/(48.2\tau_v) \pm 0.25\%$	$1/(21.40\tau_v) \pm 0.07\%$	$1/(86.2\tau_v) \pm 0.07\%$	$1/(7.95\tau_v) \pm 0.06\%$
12	0.0800	0.0600	0.1614	0.2210	0.1261	0.2857	0.0657	$1/(48.4\tau_v) \pm 0.25\%$	$1/(21.66\tau_v) \pm 0.07\%$	$1/(86.2\tau_v) \pm 0.07\%$	$1/(8.24\tau_v) \pm 0.06\%$
13	0.0	0.0	0.0	0.0	1.0	0.0	0.0	$1/(80.3\tau_v) \pm 0.28\%$	$1/(45.38\tau_v) \pm 0.07\%$	$1/(177.7\tau_v) \pm 0.07\%$	$1/(14.75\tau_v) \pm 0.04\%$
14	0.0	0.0	0.0	0.0	0.2400	0.0	0.7600	$1/(77.5\tau_v) \pm 0.27\%$	$1/(40.04\tau_v) \pm 0.07\%$	$1/(159.0\tau_v) \pm 0.07\%$	$1/(17.50\tau_v) \pm 0.04\%$
15	0.0	0.0	0.0	0.0	0.1800	0.0	0.8200	$1/(77.3\tau_v) \pm 0.13\%$	$1/(41.31\tau_v) \pm 0.07\%$	$1/(157.3\tau_v) \pm 0.07\%$	$1/(18.99\tau_v) \pm 0.04\%$
16	0.0	0.0	0.0	0.0	0.1200	0.0	0.8800	$1/(77.9\tau_v) \pm 0.23\%$	$1/(44.18\tau_v) \pm 0.07\%$	$1/(157.4\tau_v) \pm 0.07\%$	$1/(21.50\tau_v) \pm 0.05\%$
17	0.0	0.0	0.0	0.0	0.0600	0.0	0.9400	$1/(82.9\tau_v) \pm 0.07\%$	$1/(52.37\tau_v) \pm 0.07\%$	$1/(167.6\tau_v) \pm 0.08\%$	$1/(26.29\tau_v) \pm 0.05\%$
18	0.0	0.0	0.0	0.0	0.0300	0.0	0.9700	$1/(94.2\tau_v) \pm 0.19\%$	$1/(63.59\tau_v) \pm 0.08\%$	$1/(196.8\tau_v) \pm 0.08\%$	$1/(30.60\tau_v) \pm 0.06\%$
19	0.0	0.0	0.0	0.0	0.0150	0.0	0.9850	$1/(109.8\tau_v) \pm 0.13\%$	$1/(74.97\tau_v) \pm 0.08\%$	$1/(247.6\tau_v) \pm 0.06\%$	$1/(33.74\tau_v) \pm 0.06\%$
(*c*)											
20	0.0	0.0	0.0	0.0	0.0	1.0	0.0	$1/(154.8\tau_v) \pm 0.27\%$	$1/(96.91\tau_v) \pm 0.09\%$	$1/(490.7\tau_v) \pm 0.09\%$	$1/(37.96\tau_v) \pm 0.06\%$
21	0.0	0.0	0.0	0.5	0.0	0.5	0.0	$1/(112.5\tau_v) \pm 0.23\%$	$1/(59.69\tau_v) \pm 0.07\%$	$1/(271.5\tau_v) \pm 0.07\%$	$1/(21.89\tau_v) \pm 0.05\%$
22	0.0	0.3333	0.0	0.3333	0.0	0.3333	0.0	$1/(85.9\tau_v) \pm 0.21\%$	$1/(41.93\tau_v) \pm 0.08\%$	$1/(182.8\tau_v) \pm 0.04\%$	$1/(15.07\tau_v) \pm 0.04\%$
23	0.0	0.25	0.0	0.25	0.0	0.25	0.25	$1/(68.0\tau_v) \pm 0.19\%$	$1/(31.80\tau_v) \pm 0.07\%$	$1/(135.6\tau_v) \pm 0.03\%$	$1/(11.39\tau_v) \pm 0.03\%$
24	0.2	0.2	0.0	0.2	0.0	0.2	0.2	$1/(56.4\tau_v) \pm 0.18\%$	$1/(25.55\tau_v) \pm 0.07\%$	$1/(107.1\tau_v) \pm 0.03\%$	$1/(9.17\tau_v) \pm 0.03\%$
25	0.19	0.19	0.0	0.19	0.05	0.19	0.19	$1/(48.8\tau_v) \pm 0.09\%$	$1/(22.81\tau_v) \pm 0.06\%$	$1/(86.4\tau_v) \pm 0.08\%$	$1/(8.59\tau_v) \pm 0.04\%$
26	0.185	0.185	0.0	0.185	0.075	0.185	0.185	$1/(47.8\tau_v) \pm 0.26\%$	$1/(22.08\tau_v) \pm 0.06\%$	$1/(84.4\tau_v) \pm 0.08\%$	$1/(8.37\tau_v) \pm 0.04\%$
27	0.18	0.18	0.0	0.18	0.10	0.18	0.18	$1/(47.2\tau_v) \pm 0.22\%$	$1/(22.58\tau_v) \pm 0.06\%$	$1/(83.6\tau_v) \pm 0.08\%$	$1/(8.19\tau_v) \pm 0.04\%$
28	0.175	0.175	0.0	0.175	0.125	0.175	0.175	$1/(47.0\tau_v) \pm 0.26\%$	$1/(21.21\tau_v) \pm 0.07\%$	$1/(83.3\tau_v) \pm 0.03\%$	$1/(8.04\tau_v) \pm 0.03\%$
29	0.17	0.17	0.0	0.17	0.15	0.17	0.17	$1/(46.8\tau_v) \pm 0.25\%$	$1/(20.94\tau_v) \pm 0.07\%$	$1/(83.2\tau_v) \pm 0.03\%$	$1/(7.92\tau_v) \pm 0.03\%$
30	0.165	0.165	0.0	0.165	0.175	0.165	0.165	$1/(46.8\tau_v) \pm 0.24\%$	$1/(20.76\tau_v) \pm 0.07\%$	$1/(83.2\tau_v) \pm 0.07\%$	$1/(7.82\tau_v) \pm 0.05\%$
31	0.16	0.16	0.0	0.16	0.20	0.16	0.16	$1/(46.9\tau_v) \pm 0.08\%$	$1/(20.64\tau_v) \pm 0.07\%$	$1/(83.3\tau_v) \pm 0.07\%$	$1/(7.74\tau_v) \pm 0.05\%$
32	0.155	0.155	0.0	0.155	0.225	0.155	0.155	$1/(46.8\tau_v) \pm 0.21\%$	$1/(20.55\tau_v) \pm 0.07\%$	$1/(83.4\tau_v) \pm 0.07\%$	$1/(7.69\tau_v) \pm 0.05\%$
(*d*)											
33	0.17	0.17	0.05	0.17	0.10	0.17	0.17	$1/(47.6\tau_v) \pm 0.09\%$	$1/(20.81\tau_v) \pm 0.07\%$	$1/(84.9\tau_v) \pm 0.03\%$	$1/(7.74\tau_v) \pm 0.03\%$
34	0.16	0.16	0.05	0.16	0.15	0.16	0.16	$1/(47.4\tau_v) \pm 0.22\%$	$1/(20.60\tau_v) \pm 0.07\%$	$1/(84.8\tau_v) \pm 0.03\%$	$1/(7.60\tau_v) \pm 0.03\%$
35	0.155	0.155	0.05	0.155	0.175	0.155	0.155	$1/(47.5\tau_v) \pm 0.08\%$	$1/(20.54\tau_v) \pm 0.07\%$	$1/(84.8\tau_v) \pm 0.09\%$	$1/(7.55\tau_v) \pm 0.04\%$
36	0.15	0.15	0.05	0.15	0.20	0.15	0.15	$1/(47.5\tau_v) \pm 0.08\%$	$1/(20.51\tau_v) \pm 0.07\%$	$1/(84.9\tau_v) \pm 0.06\%$	$1/(7.52\tau_v) \pm 0.04\%$
37	0.145	0.145	0.05	0.145	0.225	0.145	0.145	$1/(47.6\tau_v) \pm 0.07\%$	$1/(20.51\tau_v) \pm 0.07\%$	$1/(85.0\tau_v) \pm 0.06\%$	$1/(7.51\tau_v) \pm 0.03\%$
38	0.18	0.18	0.0	0.15	0.16	0.15	0.18	$1/(46.8\tau_v) \pm 0.15\%$	$1/(20.92\tau_v) \pm 0.07\%$	$1/(83.2\tau_v) \pm 0.03\%$	$1/(7.93\tau_v) \pm 0.03\%$
39	0.16	0.16	0.0	0.19	0.14	0.19	0.16	$1/(47.0\tau_v) \pm 0.26\%$	$1/(21.09\tau_v) \pm 0.07\%$	$1/(83.3\tau_v) \pm 0.03\%$	$1/(7.97\tau_v) \pm 0.03\%$
(*e*)											
40	0.18	0.13	0.0	0.18	0.15	0.18	0.18	$1/(46.9\tau_v) \pm 0.13\%$	$1/(20.97\tau_v) \pm 0.07\%$	$1/(83.3\tau_v) \pm 0.03\%$	$1/(7.92\tau_v) \pm 0.03\%$
41	0.16	0.21	0.0	0.16	0.15	0.16	0.16	$1/(46.9\tau_v) \pm 0.24\%$	$1/(21.00\tau_v) \pm 0.07\%$	$1/(83.1\tau_v) \pm 0.03\%$	$1/(7.99\tau_v) \pm 0.03\%$
42	0.18	0.18	0.0	0.18	0.15	0.18	0.13	$1/(47.2\tau_v) \pm 0.04\%$	$1/(21.05\tau_v) \pm 0.07\%$	$1/(83.4\tau_v) \pm 0.09\%$	$1/(7.93\tau_v) \pm 0.04\%$
43	0.165	0.165	0.0	0.165	0.15	0.165	0.19	$1/(46.8\tau_v) \pm 0.09\%$	$1/(20.92\tau_v) \pm 0.07\%$	$1/(83.1\tau_v) \pm 0.09\%$	$1/(7.94\tau_v) \pm 0.04\%$
44	0.16	0.16	0.0	0.16	0.15	0.16	0.21	$1/(46.7\tau_v) \pm 0.13\%$	$1/(20.93\tau_v) \pm 0.07\%$	$1/(82.9\tau_v) \pm 0.09\%$	$1/(7.97\tau_v) \pm 0.04\%$
45	0.155	0.155	0.0	0.155	0.15	0.155	0.23	$1/(46.6\tau_v) \pm 0.09\%$	$1/(20.96\tau_v) \pm 0.08\%$	$1/(82.9\tau_v) \pm 0.07\%$	$1/(8.02\tau_v) \pm 0.03\%$
46	0.15	0.15	0.0	0.15	0.15	0.15	0.25	$1/(46.5\tau_v) \pm 0.15\%$	$1/(20.98\tau_v) \pm 0.08\%$	$1/(82.8\tau_v) \pm 0.06\%$	$1/(8.09\tau_v) \pm 0.03\%$
47	0.145	0.145	0.0	0.145	0.15	0.145	0.27	$1/(46.6\tau_v) \pm 0.15\%$	$1/(21.01\tau_v) \pm 0.07\%$	$1/(82.7\tau_v) \pm 0.06\%$	$1/(8.17\tau_v) \pm 0.03\%$
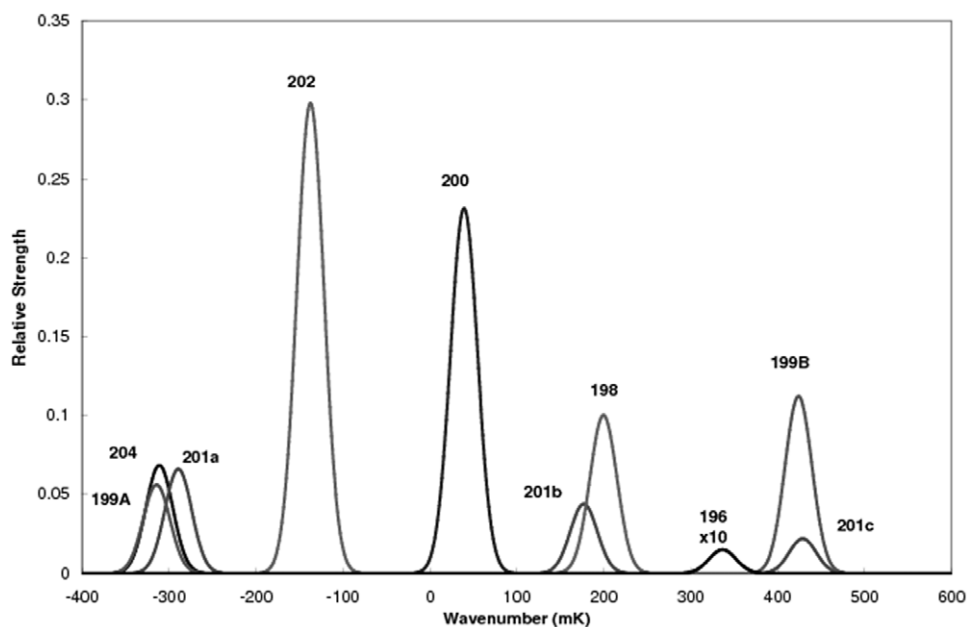
Figure 1. Component pattern of the 253.7 nm Hg line as a function of wavenumber (1 mK$=$ 0.001 cm^{-1}). Isotopic components are identified. The line shape and width corresponds to Doppler broadening at 335 K.

temperature), a Hg density 1.88×10^{14} cm^{-3}, and an operating gas temperature of 335 K. Simulations in rows 36–37 of table 1(*d*) yield the best result for the T5 column with an escape rate of 120% of that in row 1 of table 1(*a*) for a natural isotopic mix and 103% of that in row 8 of table 1(*a*) for an optimum addition of the ^{196}Hg isotope to a natural isotopic mix. The lower opacity of the small diameter lamps does shift the optimum escape rate for Hg 254 nm resonance radiation to a somewhat different isotopic mix. The shift of the optimum mix from row 46 of table 1(*e*) for a T12 lamp to rows 36–37 of table 1(*d*) for T5 lamp is confirmed in studies of the T16 and T2 lamps described below.

Results from simulations in the Electrodeless(T16) or 50 mm diameter column are for an Ar buffer gas density of 9.88×10^{15} cm^{-3}, (0.30 Torr at 293 K fill temperature), and a Hg density of 1.88×10^{14} cm^{-3}, and an operating gas temperature of 335 K. This larger diameter system operating at lower pressure is much like the ICETRON/ENDURA lamps of Osram Sylvania Inc. These electrodeless products represent some of the largest diameter lamps on the market today. The simulation in row 47 of table 1(*e*) yields the best result of the Electrodeless(T16) column with an escape rate 121% of that in row 1 of table 1(*a*) for a natural isotopic mix and 104% of that in row 6 of table 1(*a*) for an optimum addition of the ^{196}Hg isotope to a natural isotopic mix. The electrodeless ICETRON/ENDURA lamps Osram Sylvania Inc. operate at appreciably higher current ($\sim$7 A) than electroded fluorescent lamps. This higher current is needed to optimize the lamp efficiency by lowering losses in the ferrite cores used to couple radio frequency power into the lamp discharge (Godyak *et al* 1998). The larger diameter of these lamps results in generally lower escape rates for Hg 254 nm resonance radiation. The higher power density may result in higher rates for inelastic and super-elastic electron Hg atom collisions. For example, it is known that the ratio of Hg resonance radiation at 185 nm

to that at 254 nm is higher in such discharges than standard fluorescent lamps (Menningen and Lawler 2000). The increase in the ratio of 185 to 254 nm radiation reaching the phosphor degrades lamp performance because of the larger Stokes shift to the visible and because the more energetic 185 nm photons tend to shorten the phosphor life. A larger diameter, higher power density discharge is an ideal test case for a customized Hg isotopic mix. The overall improvement in lamp efficacy may be higher in larger diameter, high power density lamps than the 4% efficacy improvement found by Grossman *et al* (1986) for a standard electroded T12 lamp.

Results from simulations in the Miniature(T2) or 6.4 mm diameter column are for an Ar buffer gas density of 1.65×10^{17} cm^{-3}, (5 Torr at 293 K fill temperature) a Hg density 1.88×10^{14} cm^{-3}, and an operating gas temperature of 335 K. Small diameter Miniature or T2 (1/4 inch diameter) lamps are specialty products available from many manufacturers and such products are used for back lighting displays and in other applications were space is limited. These small diameter T2 lamps have generally higher escape rates for Hg 254 nm resonance radiation than T8, T12 and large diameter electrodeless (T16 or T17) lamps discussed above. Small diameter lamps do tend to operate at higher power density than Standard 4 ft. fluorescent lamps used for general illumination. Many compact fluorescent lamps have tube diameters similar to T2 lamps or between that of T2 lamps and the widely used Standard (T12 or T8) 4 ft. long tubular lamps. The simulation in row 37 of the Miniature column in table 1(*d*) yields the best result of that column with an escape rate 122% of that in row 1 of table 1(*a*) for a natural isotopic mix and 103% of that in row 9 of table 1(*a*) for an optimum addition of the ^{196}Hg isotope to a natural isotopic mix.

Our study included many additional Monte Carlo simulations that are not reported in table 1. However, the results in table 1 are representative. The above results indicate

that the optimum isotopic mix is somewhat dependent on lamp diameter and/or buffer gas density. The efficiency of the MAGIS isotope separation technique opens the possibility of customizing the Hg isotopic mix for particular lamp designs. Our numerical studies explore only the escape rate of Hg 254 nm resonance radiation. Increases in lamp efficacy need to be measured under realistic operating conditions. Numerical modelling the fluorescent lamp discharges is valuable, for example in helping understand trends. The lack of accurate and precise atomic collision data for many important multi-step processes involving excited atoms is a serious impediment to using discharge models to assess the efficacy increase from an enhanced 254 nm escape rate. Nevertheless some attempt at modelling complete fluorescent lamp discharges with isotopically tailored Hg doses is worthwhile. If there were no quenching collisions then the steady-state number of resonance $6s6p\,^3P_1$ atoms would be their excitation rate divided by the 254 nm escape rate. With no quenching collisions the lamp efficacy would be independent of the escape rate! If the rate of quenching collisions was large compared to the 254 nm escape rate, then the lamp efficacy would improve in proportion to the 254 nm escape rate. Of course such a high quenching rate is inconsistent with the high, ∼60% to 70%, UV power efficiency of a fluorescent lamp discharge. Quenching collisions do convert the electronic excitation energy of some $6s6p\,^3P_1$ atoms into gas heat, wall heat, or ionization and thus degrade lamp efficacy. Not all multi-step processes reduce lamp efficacy. For example, a multi-step process including electron impact excitation from the resonance $6s6p\,^3P_1$ level to the $6s7s\,^3S_1$ level, followed by emission of a 546 nm photon, and subsequently followed by one or more collisions to de-excite the atom from the metastable $6s6p\,^3P_2$ level to the resonance $6s6p\,^3P_1$ level enhances lamp efficacy. Knowledge of the cross sections and/or rate constants for multi-step processes involving excited atoms is not adequate. Although modelling typically provides both guidance and interpretation of experiments, measurements are needed to assess the efficacy increase from an enhanced 254 nm escape rate. An increase of ∼20% in the escape rate of Hg 254 nm radiation, a process that dominates the power balance of the lamp, is large enough to appreciably perturb the plasma. Some re-optimization of lamp parameters should be explored.

5. Summary and future tasks

The simulations revealed that a natural isotopic mix is relatively well balanced except for a shortage of the rare ^{196}Hg isotope. Modest improvements, beyond what can be done just be adding ^{196}Hg, are possible in the radiation escape rate under typical fluorescent lamp conditions by completely re-optimizing the isotopic mix. In a 38 mm diameter lamp we found an isotopic mix that yields an increase of 17% in the radiation escape rate over that occurring with a natural isotopic mix and 4% over the best rate achieved by simply adding ^{196}Hg. Somewhat larger improvements of 20% in a 15.9 mm diameter lamp, 21% in a 50 mm diameter lamp, and 22% in 6.4 mm diameter lamp are found. These 17% to 22% enhancement of the UV resonance radiation escape rate are

sufficiently large that it should be worthwhile re-optimizing lamp operating conditions, including the Hg density or cold spot temperature, buffer gas density, and discharge current density. We suggest that the large diameter, low pressure electrodeless lamps operating at high power density may benefit the most from an optimized isotopic mix.

The most urgent task ahead is to demonstrate that MAGIS can separate Hg isotopes for very low costs. When that is demonstrated then numerical modelling and especially experimental studies of fluorescent lamps with tailored isotopic mixes become a priority. The experimental studies should explore re-optimization of lamp parameters. If a 10% to 15% improvement in lamp efficacy is both possible and economically viable, the application of these ideas to ultra-long lived electrodeless fluorescent lamps may be the most logical next step. These radio frequency driven lamps are expensive and the incremental cost of a tailored isotopic mix may be negligible compared to the lamp plus ballast cost. The longer term goal is of course to improve the efficacy of the very widely used standard T8 or T5 4 ft. long fluorescent lamp.

References

Anderson H M, Bergeson S D, Doughty D A and Lawler J E 1995 *Phys. Rev. A* **51** 211
Anderson J B, Maya J, Grossman M W, Lagushenko R and Waymouth J F 1985 *Phys. Rev. A* **31** 2968
Benck E C, Lawler J E and Dakin J T 1989 *J. Opt. Soc. Am. B* **6** 11
Biberman L M 1947 *Zh. Eksp. Toer. Fiz.* **17** 416
Böhlke J K, de Laeter, J R, De Bièvre P, Hidaka H, Peiser H S, Rosman, K J R and Taylor P D P 2005 *J. Phys. Chem. Ref. Data* **34** 57
Bousquet C and Bras N 1980 *J. Phys. Fr.* **41** 19
Corney A 1977 *Atomic and Laser Spectroscopy* (Oxford: Clarendon) p 263
Gerstenkorn S, Labarthe J J and Verges J 1977 *Phys. Scr.* **15** 167
Godyak V A, Alexandrovich B, Piejak R B and Statnic E 1998 *US Patent* 5,834,905
Grossman M W, Lagushenko R and Maya J 1986 *Phys. Rev. A* **34** 4094
Herd M T, Lawler J E and Menningen K L 2005 *J. Phys. D: Appl. Phys.* **38** 3304
Holstein T 1947 *Phys. Rev.* **72** 1212
Lawler J E, Parker G J and Hitchon W N G 1993 *J. Quant. Spectrosc. Radiat. Transfer* **49** 627
Lee J-S 1974 *Astrophys. J.* **192** 465
Lee J-S 1977 *Astrophys. J.* **218** 857
Lee J-S 1982 *Astrophys. J.* **255** 303
Menningen K L and Lawler J E 2000 *J. Appl. Phys.* **88** 3190
Molisch A F and Oehry B P 1998 *Radiation Trapping in Atomic Vapors* (Oxford: Clarendon)
Parker G J, Hitchon W N G and Lawler J E 1993 *J. Phys. B.: At. Mol. Opt. Phys.* **26** 4643
Paul J, Kaneda Y, Wang, T, Lytle C, Moloney J V and Jones R J 2011 *Opt. Lett.* **36** 61
Perrin D and Jeannet J C 1981 *J. Phys. Fr.* **42** 1607
Raizen M G and Klappauf B 2012 *New J. Phys.* **14** 023059
Schweitzer W G 1963 *J. Opt. Soc. Am* **53** 1055
Von Neumann J 1951 *US Natl. Bur. Stand. Appl. Math. Ser.* **12** 36
Work D E and Johnson S G 1983 *US Patent* 4,379,252